Nonlinear Rheology in a Model Biological Tissue

D. a. Matoz-Fernandez, Elisabeth Agoritsas, Jean-Louis Barrat, Eric Bertin, Kirsten Martens

Nonlinear Rheology in a Model Biological Tissue

D. A. Matoz-Fernandez,[1,*] Elisabeth Agoritsas,[1,2,†] Jean-Louis Barrat,[1] Eric Bertin,[1] and Kirsten Martens[1]

[1] *Université Grenoble Alpes & CNRS, LIPHY, F-38000 Grenoble, France*
[2] *Laboratoire de Physique Théorique, ENS & PSL University, UPMC & Sorbonne Universités, F-75005 Paris, France*

The rheological response of dense active matter is a topic of fundamental importance for many processes in nature such as the mechanics of biological tissues. One prominent way to probe mechanical properties of tissues is to study their response to externally applied forces. Using a particle-based model featuring random apoptosis and environment-dependent division rates, we evidence a crossover from linear flow to a shear-thinning regime with an increasing shear rate. To rationalize this nonlinear flow we derive a theoretical mean-field scenario that accounts for the interplay of mechanical and active noise in local stresses. These noises are, respectively, generated by the elastic response of the cell matrix to cell rearrangements and by the internal activity.

Mechanical stimuli on single cells [1] and cell assemblies [2] play an important role in biology, for example in the mechanics of biofilms [3] as well as for medical issues [4, 5]. Furthermore, mechanical sensing has been shown to be of vital importance in cancer growth [6–8] and morphogenesis [9, 10]. Driven by advances in experimental cell tracking techniques [11–14], this topic has gained a lot of importance in recent years. The mechanical response of cell aggregates under deformation has been shown to exhibit elastic, elastoplastic and viscous flow behavior depending on the forces applied and the time scale of observation considered [12, 15, 16]. Recently there have been many efforts to understand the origin of these different mechanical regimes. It has been shown that both self-propulsion [17–20], as well as cell division and apoptosis [21–23] are processes able to fluidize a confluent cell assembly, which appears to be arrested in a glassy configuration otherwise.

In this Letter we go beyond the study of the specific fluidization mechanism and the corresponding linear flow regime [22]. We investigate the flow properties of a confluent tissue under shear using a particle-based model that incorporates activity in the form of cell division and apoptosis [23]. We find that the internal activity gives rise to a fluidization of the tissues at shear rates smaller than a time scale set by the apoptosis rate, followed by a shear-thinning regime, well described by a Herschel-Bulkley flow curve at higher shear rates. These findings are in agreement with experimental studies on epithelial cell monolayers [14], which showed that the structural relaxation time of their tissue was purely governed by the cell division time in the high density regime.

In analogy to the flow of soft matter, such as emulsions or foams, we propose a statistical description to derive an analytical prediction for the complex flow curve in confluent tissues. At the core of this description is an elastoplastic picture: the inactive cell assembly responds elastically to external forcing like a solid up to a threshold above which it is able to locally yield through cell-cell rearrangements leading to plastic flow as shown in the stress-strain curve in the bottom panel of Fig. 1.

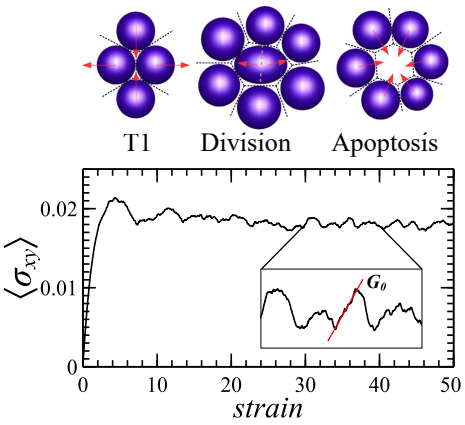

FIG. 1. (*Top*) Microscopic events in a system with cell division and apoptosis under shear. From left to right, T1 event (passive rearrangement), cell division and apoptosis (active rearrangements). (*Bottom*) Typical macroscopic stress-strain curve, the average slope of the increasing elastic parts on the curve corresponds to the elastic modulus G_0.

The local rearrangements (T1 events, see sketch in Fig. 1) lead to a long-range elastic response of the surrounding medium that will create a mechanical noise [24]. We argue that the elastic perturbation created through the internal activity, for example via cell division and apoptosis (sketch in Fig. 1), creates an additional active noise. The interplay of these different mechanisms leads to an interesting nontrivial flow behavior. We rationalize these findings using a mean-field description that extends the Hébraud-Lequeux model [25] of athermal yield stress fluids.

In spite of the inherent complexity of tissue mechanics, many interesting collective phenomena at tissue level can be described using simple models in which cell-cell interactions are treated as soft interactions between particles [26, 27]. In this spirit, we model a tissue as a collection of N soft spherical particles with radii b_i uniformly distributed in a range of 0.85 to 1.15. Moreover, in order to mimic the real behavior of cells in epithelial sheets we

consider adhesion and excluded volume as a combination of attractive and repulsive forces [23, 28],

$$\mathbf{F}_{ij} = \begin{cases} -kb_{ij}\left(1 - \frac{r_{ij}}{b_{ij}}\right)\hat{\mathbf{r}}_{ij} & \text{if } 0 \le \frac{r_{ij}}{b_{ij}} \le \epsilon + 1 \\ kb_{ij}\left(2\epsilon + 1 - \frac{r_{ij}}{b_{ij}}\right)\hat{\mathbf{r}}_{ij} & \text{if } \epsilon < \frac{r_{ij}}{b_{ij}} - 1 \le 2\epsilon, \end{cases} \quad (1)$$

where k is the stiffness constant, $b_{ij} = b_i + b_j$ is the sum of the particle radii and ϵ is the ratio of the maximal attractive and maximal repulsive forces. The cell centroids $\mathbf{r}_i(t)$ follow an overdamped dynamics, $\partial_t \mathbf{r}_i(t) = \mu \mathbf{F}_i$, where μ is the mobility coefficient [29]. In addition, activity is introduced via apoptosis and cell-division rates. Apoptosis (as well as possibly other cell death mechanisms) is included by removing cells randomly at a constant rate a. On the other hand, as in real epithelial tissues, the contact inhibition process [30] is modeled via a density-dependent division rate $d_i = d_0(1 - z_i/z_{\max})$, with d_0 the division rate amplitude, z_i the number of contact neighbors of particle i, and $z_{\max}$ the maximum number of contact neighbors allowed. After any division, the new daughter cell is placed on top of the mother cell. In order to prevent any numerical instability, the total force exerted by the mother and daughter cells on the surrounding cells is kept continuous, by applying only half the force immediately after cell division, and then progressively increasing the applied force to reach again a nominal force applied on each cell [23].

We carried out 2D simulations of the model with fixed values $z_{\max} = 6$, $\epsilon = 0.05$ [31]. By setting $\mu = k = 1$ we set the unit time to the elastic relaxation time $\tau_{\rm el} = (\mu k)^{-1}$, typically of the order of minutes [15]. We take as a control parameter the apoptosis rate a, where a^{-1} is in experiments of the order of half an hour to half a day [14, 32]. Since varying a at the fixed maximal division rate d_0 would lead to large variations in packing fraction, we rather fix d_0 through the relation $a/d_0 = 0.1$ (consistent with the choice of the other parameters and typical experimental values [14]), leading to limited changes of the packing fraction.

After a steady state has been reached in the absence of shear, with the average division rate balancing the apoptosis rate, we impose a constant shear rate $\dot\gamma$ via deformation of a triclinic box with periodic boundary conditions. We apply a strain of more than 10 to ensure that the steady state has been reached and measure the macroscopic shear stress $\sigma_{xy}(t)$ as illustrated in Fig. 1.

We have established that the homeostatic properties of the system do not strongly depend on a [31]. For low enough shear rate $\dot\gamma$ and apoptosis rate a, the packing fraction is constant [Fig. 2(b)]. A careful analysis of the packing fraction Φ as a function of a and $\dot\gamma$ [Fig. 2(b)] however reveals two different regimes in which the packing fraction deviates from this constant value. First, considering a fixed low shear rate (typically $\dot\gamma < 10^{-3}$), the packing fraction Φ increases with activity if $a \gtrsim 10^{-3}$.

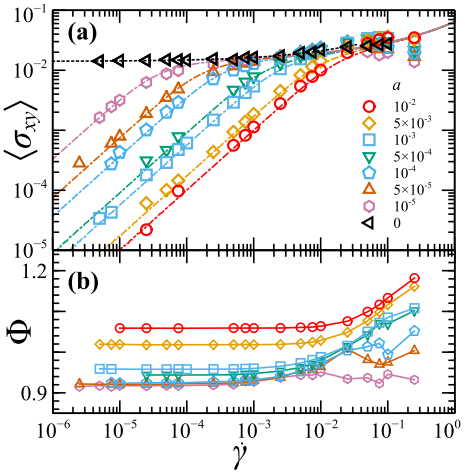

FIG. 2. *Flow curves for passive and active systems* – (a) Steady-state average shear stress $\langle\sigma_{xy}\rangle$ versus the applied external shear rate $\dot\gamma$ for different apoptosis rates a. The symbols indicate the microscopic simulations results for the different apoptosis rates. The dashed line corresponds to a Herschel-Bulkley fit of the passive system with packing fraction $\Phi \approx 0.94$. The dashed-dotted lines are the mean-field model fits with fitting parameter D_0. (b) Shear-rate dependence of the corresponding packing fraction Φ for the same values of the apoptosis rates.

This is understood as an interplay between the division rate d_0 (equal to $0.1a$) and the mechanical relaxation rate μk in the soft repulsive potential [23]. As long as the elastic relaxation time $\tau_{\rm el} = (\mu k)^{-1}$ remains small with respect to the typical time $\tau_{\rm a} = (d_0)^{-1}$ between two divisions involving the same cell, the elastic relaxation processes remain independent and the packing fraction remains constant. When, in constrast, $\tau_{\rm a} \ll \tau_{\rm el}$, multiple divisions occur during the elastic relaxation, and the resulting packing fraction depends on the activity a. The second regime is related to the effect of a strong enough shear rate, typically $\dot\gamma > 10^{-3}$. In this case, we observe that a fast and large deformation of the box produces a rapid decrease of the number of contact neighbors followed by an increase of the division rate, eventually leading to a steady state with a higher packing fraction.

The corresponding flow curves, i.e., the steady-state macroscopic stress $\langle\sigma_{xy}\rangle$ as a function of $\dot\gamma$, are shown in Fig. 2(a) for different values of the apoptosis rate. In the absence of activity ($a = 0$) the system exhibits a nonlinear rheology as observed in foams; it is well known that this type of dynamics is then characterized at low shear rates by a Herschel-Bulkley flow curve $\langle\sigma_{xy}\rangle = \sigma_y^{(d)} + A_{\rm HB}\dot\gamma^n$. In other words, in the limit of zero shear rate, the macroscopic stress takes a finite value, known as the dynamical yield stress $\sigma_y^{(d)}$, and then increases with the shear rate following a power-law behavior [33]. In our case, we obtain $\sigma_y^{(d)} = 0.014$,

$A_{\rm HB} = 0.065$ and $n \approx 0.5$ for $\dot\gamma \leq 0.025$ (see the dashed curve), this exponent being consistent with those observed in foams and in recent molecular dynamics simulations [24]. On the other hand, a finite activity $a > 0$ prevents the system from having a finite yield stress $\sigma_y^{(d)}$, leading to a linear behavior at low shear rates, with a viscosity that decreases when a increases. Here the new feature is the crossover, at a shear rate $\dot\gamma^*$ controlled by the activity, from a Newtonian to a Herschel-Bulkley behavior. Defining the crossover as the intersection between the linear regime and the plateau, we have plotted $\dot\gamma^*(a)$ in Fig. 3(b), obtaining an almost linear dependence $\dot\gamma^* \sim a^{0.82}$. We emphasize that, at least for small enough activity ($a \lesssim 10^{-4}$), the crossover from activity-driven fluidization to a yield-stress (plateau) behavior occurs at a constant packing fraction. On the contrary, the stress increase at large shear rate $\dot\gamma$ results from both standard elastoplastic effects and the increase of the packing fraction.

The crossover from linear to nonlinear flow behaviors of the sheared active system can be captured via a minimal mean-field description that focuses on the dynamics of the local shear stress. For this purpose, we use an athermal-local-yield-stress model [34, 35], which generalizes the original Hébraud-Lequeux model [25]. These models usually do not take into account any active contribution to the local stress fluctuations. As shown in Fig. 2(a), this active contribution is however a key ingredient for fluidizing the system and is thus introduced explicitly thereafter. In a simplified mean-field picture, the dynamics of the local stress can be modeled by a modified Langevin dynamics, $\partial_t \sigma(t) = G_0 \dot\gamma + \xi_{\rm mec}(t)$ with G_0 the average local elastic modulus, $\dot\gamma$ the external constant shear rate, and $\xi_{\rm mec}(t)$ the mechanical noise. In addition, once $\sigma(t)$ exceeds a typical threshold σ_c, a local plastic event randomly occurs at a fixed rate $1/\tau$, which would in turn fully relax the local stress and thus reset $\sigma(t)$ to 0. Here, $\xi_{\rm mec}(t)$ is modeled by a Gaussian noise with zero mean. Furthermore, at the time scale we consider, we can neglect its time correlation, i.e., $\langle \xi_{\rm mec}(t)\xi_{\rm mec}(t')\rangle = 2D(t)\delta(t-t')$, where the brackets corresponds to average over time, and $D(t)$ is the stress diffusion coefficient. At low shear rate, a natural way to introduce activity is to distinguish two contributions to the noise, i.e., $\xi_{\rm mec}(t) = \xi_{\rm pl}(t) + \xi_{\rm act}(t)$. The noise $\xi_{\rm pl}(t)$ accounts for the plastic events triggered by the external driving throughout the system, and has a time-dependent diffusion coefficient $D_{\rm pl}(t)$. The noise $\xi_{\rm act}(t)$ corresponds to the stress fluctuations produced by activity (cell division and apoptosis), and has a time-independent diffusion coefficient D_0. We assume that these two competing noises are statistically independent. Hence, the stress diffusion coefficient has two additive contributions, $D(t) = D_{\rm pl}(t) + D_0$. Following the standard Hébraud-Lequeux model [25], the diffusion coefficient $D_{\rm pl}(t)$ modeling the effect of plastic events is self-

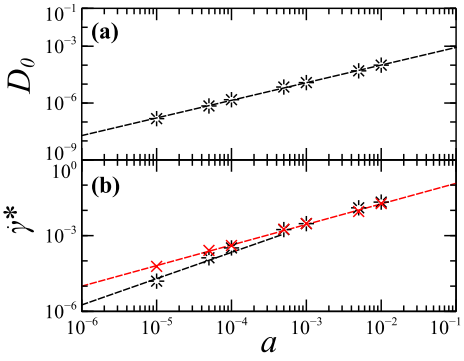

FIG. 3. (a) Fitted value of the diffusion coefficient D_0 of the active noise as a function of the apoptosis rate a from the mean-field fit on the simulation data. The dashed line is a power-law fit with an exponent 0.94. (b) Activity-dependent crossover shear rate $\dot\gamma^*(a)$ measured from the flow curves (see text for details). Crosses are determined values from the pure simulation data, whereas stars come from the mean-field fit of the simulations.

consistently determined as $D_{\rm pl}(t) = \alpha\,\Gamma(t)$, where $\Gamma(t)$ is the global plastic activity and α is a coupling parameter related to the elastic stress propagator [31, 34, 36]. Here, we emphasize that the new key ingredient is the diffusion coefficient $D_0 > 0$ stemming from activity. The macroscopic stress $\langle \sigma_{xy}\rangle$ can be obtained from the probability distribution of the local stress σ. The evolution equation of this distribution is

$$\begin{aligned}\partial_t \mathcal{P}(\sigma,t) = &- G_0\dot\gamma\,\partial_\sigma \mathcal{P} + (\alpha\,\Gamma(t) + D_0)\;\partial_\sigma^2 \mathcal{P} \\ &-\frac{1}{\tau}\theta(|\sigma| - \sigma_c)\,\mathcal{P} + \Gamma(t)\,\delta(\sigma)\end{aligned} \tag{2}$$

where $\Gamma(t) = \frac{1}{\tau}\int_{|\sigma|>\sigma_c} d\sigma\,\mathcal{P}(\sigma,t)$ is the average number of sites that yield per unit time; $\Gamma(t)$ is proportional to the number of sites that have reached the threshold (i.e., $|\sigma_i| > \sigma_c$) divided by the "lifetime" τ [25, 34]. The stress on these sites is reset to zero after the yield event. These simple rules do not correspond to the true local relaxation processes [24]. The aim is to introduce the simplest analytically solvable mean-field scenario that predicts qualitatively well the numerical data with a set of few meaningful effective parameters.

In the steady state at constant shear rate, and in the absence of activity ($D_0 = 0$), it is well known that this mean-field model predicts the existence of a Herschel-Bulkley regime with an exponent $n = 1/2$ at low $\dot\gamma$ and for $\alpha < \sigma_c^2/2$ [25, 34, 35].

In the presence of activity ($D_0 > 0$), the present mean-field model reproduces the fluidization process leading to a linear behavior (i.e., Newtonian regime) and, quite importantly, recovers a nonlinear flow curve beyond a

crossover shear rate $\dot{\gamma}^*$,

$$\langle \sigma_{xy} \rangle \approx \begin{cases} \eta\,\dot{\gamma} & \text{if } \dot{\gamma} < \dot{\gamma}^* \\ \sigma_y + A_{\rm HB}\,\dot{\gamma}^{1/2} & \text{if } \dot{\gamma} > \dot{\gamma}^* \end{cases} \tag{3}$$

as observed in Fig. 2. Analytical calculations show that $\dot{\gamma}^* \sim D_0$ for $D_0 \to 0$. The explicit expressions for $\{\eta, \sigma_y, A_{\rm HB}, \dot{\gamma}^*\}$ can be computed as a function of the model parameters $\{G_0, \tau, \sigma_c, \alpha, D_0\}$, using the methods described in Ref. [34] – see the Supplemental Material in Ref. [31].

To compare the mean-field model with the numerical data of the particle-based model, we have to fit the values of the model parameters $\{G_0, \tau, \sigma_c, \alpha, D_0\}$. We used the following fitting procedure. First, the elastic modulus G_0 is estimated independently from the initial elastic response in the stress-strain curve (see Fig. 1) yielding $G_0 \approx 0.25$. Second, the parameters $\{\tau, \sigma_c, \alpha\}$ are fitted on the flow curve obtained in the absence of activity ($a = 0$, $\Phi \approx 0.94$), in turn yielding $\tau = 0.12$, $\sigma_c = 0.15$, and $\alpha = 0.45\sigma_c^2$. Having fixed the four parameters $\{G_0, \tau, \sigma_c, \alpha\}$, we then fit the different flow curves obtained in the active case ($a > 0$) with D_0 as the only free parameter. The procedure eventually yields the fitted value $D_0(a)$, which is plotted in Fig. 3(a). As expected, the fitted value of σ_c is larger than σ_y, see Eq. 3, and that the coupling α is smaller than $\sigma_c^2/2$ as required to observe a Herschel-Bulkley behavior. We further observe that the obtained value of α/σ_c^2 is larger than for the Lennard-Jones systems [24]; this larger value might be linked to the presence of a softer potential. More importantly, the stress diffusion coefficient $D_0(a)$ fitted from the mean-field prediction is plotted in Fig. 4(a), and scales fairly linearly with a. This can be understood as follows. At low a, apoptosis events are rare and independent, so we can safely assume that the typical redistributed stress $\Delta\sigma$ after such events will depend only on the packing fraction but not on the activity. Moreover, at low shear rates the only relevant time scale is set by the apoptosis rate. Thus, we can estimate the stress diffusion coefficient D_0 by a simple scaling argument as $D_0 \sim (\Delta\sigma)^2 a$. Furthermore, the mean-field picture predicts a crossover $\dot{\gamma}^*$ linear with D_0, and hence we expect $\dot{\gamma}^* \sim a$, consistently with the flow curve crossover shown in Fig. 3(b).

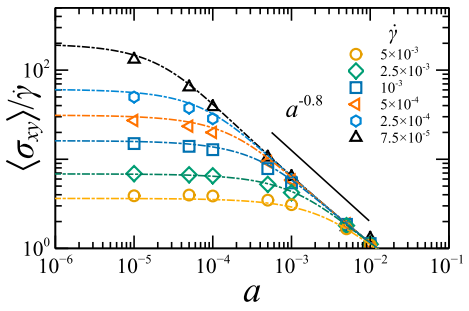

FIG. 4. Viscosity $\eta = \langle\sigma_{xy}\rangle/\dot{\gamma}$ as a function of the apoptosis rate a for different small values of the shear rate (symbols for the numerical data and dash-dotted lines for the mean-field prediction).

To provide further insights on the behavior of our model, we show in Fig. 4 the activity-dependent viscosity $\eta = \langle\sigma_{xy}\rangle/\dot{\gamma}$ for different fixed, low values of the shear rate. We observe that the viscosity decreases when the activity is enhanced beyond a (strain-rate-dependent) threshold value, i.e., fluidizing the system as previously reported in Ref. [21]. However, the Maxwell picture proposed in Ref. [21] cannot capture the crossover to the nonlinear rheology that we observe in Fig. 2(a). This is due to the fact that the plateau in the viscosity observed at low activity [see Fig. 4] does not correspond to a Newtonian regime (in which the shear stress varies linearly with $\dot{\gamma}$), but rather to a yield stress fluid behavior. This is clearly seen from the fact that the plateau value of the viscosity strongly depends on the strain rate $\dot{\gamma}$, a property that cannot be accounted for by a simple Maxwell model. The data presented in Fig. 4 can be understood as follows. At low enough activity, plasticity is dominant and the shear stress remains independent of activity. For a fixed shear rate, the viscosity $\eta = \langle\sigma_{xy}\rangle/\dot{\gamma}$ is thus independent of activity, yielding the plateau in Fig. 4. At a higher activity, the active contribution to the mechanical noise instead becomes dominant, thus decreasing the viscosity. In this regime, the mean-field model predicts $\eta \sim 1/D_0$ (see the Supplemental Material in Ref. [31]), in good agreement with Fig. 4 (dashed-dot lines), taking into account $D_0 \sim a$. Note here again the good agreement between the mean-field model and the numerical simulations.

In conclusion, we proposed in this Letter a generic scenario to understand the crossover from linear to nonlinear rheology in flowing active tissues, based on stress fluctuations mediated by long-range elastic interactions. The mean-field picture presented here allows us to introduce explicitly the interplay of the two relevant time scales in these systems, one imposed by the external shear and another by the internal processes of the biological tissue in the form of cell division and apoptosis. This scenario is able to rationalize well the numerical findings of our particle-based model for the active confluent tissue under shear, as can be seen from the flow curves and the activity-dependent viscosity.

It has been shown that our mean-field predictions are qualitatively robust to the addition of disorder [34], the partial relaxation of stress or the effective shear-rate dependence of the elastic modulus or relaxation time [35], assessing furthermore the generality of our scenario. Moreover, the introduction of additional relaxation mechanisms like cell-shape fluctuations, self propulsion, external vibrations, and other sources of mechani-

cal noise, can be easily implemented in our mean-field description via assumptions on the distribution of the active part of the noise. However, to allow for a more refined description of the dynamics aiming for a quantitative agreement, it would be interesting to investigate in more details the long-range elastic effects of cell division and apoptosis events. A strong point of our approach is that it can be easily generalized to describe the rheological response of other systems that include an additional shear-rate independent noise, such as vibrated grains [37–40], active colloidal suspensions [41] or coarsening foams [42, 43].

Acknowledgements. J.-L. B., D. A. M.-F. and E. A. acknowledge financial support from European Research Council Grant No. ADG20110209; E. A. was also supported by the Swiss National Science Foundation Grant No P2GEP2-15586 and by a Simons Foundation Grant (♯ 454955, Zamponi). J.-L. B., D. A. M.-F., and K. M. thank the NVIDIA Corporation for a hardware grant through the Academic Partnership Program. Further, we would like to thank Silke Henkes and Rastko Sknepnek for valuable discussions on the particle model description during this work.

D. A. M.-F. and E. A. contributed equally to this work.

* daniel-alejandro.matoz-fernandez@univ-grenoble-alpes.fr
† elisabeth.agoritsas@lpt.ens.fr

[1] E. Moeendarbary and A. R. Harris, Wiley Interdisciplinary Reviews: Systems Biology and Medicine **6**, 371 (2014).
[2] T. Lecuit and P.-F. Lenne, Nature Reviews. Molecular Cell Biology **8**, 633 (2007).
[3] N. Billings, A. Birjiniuk, T. S. Samad, P. S. Doyle, and K. Ribbeck, Reports on Progress in Physics **78**, 036601 (2015).
[4] C. R. Jacobs, H. Huang, and R. Y. Kwon, Introduction to Cell Mechanics and Mechanobiology (Garland Science, 2013).
[5] A. van den Berg and L. Segerink, eds., Microfluidics for Medical Applications, RSC Nanoscience & Nanotechnology (The Royal Society of Chemistry, 2015) pp. P001–303.
[6] M. J. Paszek, N. Zahir, K. R. Johnson, J. N. Lakins, G. I. Rozenberg, A. Gefen, C. A. Reinhart-King, S. S. Margulies, M. Dembo, D. Boettiger, et al., Cancer Cell **8**, 241 (2005).
[7] M. Delarue, F. Montel, D. Vignjevic, J. Prost, J.-F. Joanny, and G. Cappello, Biophysical Journal **107**, 1821 (2014).
[8] A. Nagelkerke, J. Bussink, A. E. Rowan, and P. N. Span, Seminars in Cancer Biology **35**, 62 (2015), Complexity in Cancer Biology.
[9] M. Popovic, A. Nandi, M. Merkel, R. Etournay, S. Eaton, F. Jülicher, and G. Salbreux, "Active dynamics of tissue shear flow," arXiv:1607.03304 (2016).
[10] R. Etournay, M. Popović, M. Merkel, A. Nandi, C. Blasse, B. Aigouy, H. Brandl, G. Myers, G. Salbreux, F. Jülicher, et al., Elife **4**, e07090 (2015).
[11] X. Trepat, M. R. Wasserman, T. E. Angelini, E. Millet, D. A. Weitz, J. P. Butler, and J. J. Fredberg, Nature Physics **5**, 426 (2009).
[12] T. E. Angelini, E. Hannezo, X. Trepat, M. Marquez, J. J. Fredberg, and D. A. Weitz, Proceedings of the National Academy of Sciences **108**, 4714 (2011).
[13] R. Etournay, M. Merkel, M. Popović, H. Brandl, N. A. Dye, B. Aigouy, G. Salbreux, S. Eaton, and F. Jülicher, Elife **5**, e14334 (2016).
[14] K. D. Nnetu, M. Knorr, S. Pawlizak, T. Fuhs, and J. A. Käs, Soft Matter **9**, 9335 (2013).
[15] P. Marmottant, A. Mgharbel, J. Kaefer, B. Audren, J.-P. Rieu, J.-C. Vial, B. van der Sanden, A. F. M. Marée, F. Graner, and H. Delanoe-Ayari, Proceedings of the National Academy of Sciences **106**, 17271 (2009).
[16] S. Heermann, L. Schütz, S. Lemke, K. Krieglstein, and J. Wittbrodt, Elife **4**, e05216 (2015).
[17] L. Berthier, Physical Review Letters **112**, 220602 (2014).
[18] R. Mandal, P. J. Bhuyan, M. Rao, and C. Dasgupta, Soft Matter **12**, 6268 (2016).
[19] D. Bi, X. Yang, M. C. Marchetti, and M. L. Manning, Physical Review X **6**, 021011 (2016).
[20] G. Szamel, E. Flenner, and L. Berthier, Physical Review E **91**, 062304 (2015).
[21] J. Ranft, M. Basan, J. Elgeti, J.-F. Joanny, J. Prost, and F. Jülicher, Proceedings of the National Academy of Sciences **107**, 20863 (2010).
[22] M. Basan, J. Prost, J.-F. Joanny, and J. Elgeti, Physical Biology **8**, 026014 (2011).
[23] D. Matoz Fernandez, K. Martens, R. Sknepnek, J. L. Barrat, and S. Henkes, "Fluidization of tissues due to cell division and apoptosis," arXiv:161 [cond-mat.soft] (2016).
[24] F. Puosi, J. Olivier, and K. Martens, Soft Matter **11**, 7639 (2015).
[25] P. Hébraud and F. Lequeux, Physical Review Letters **81**, 2934 (1998).
[26] D. Drasdo, S. Hoehme, and M. Block, Journal of Statistical Physics **128**, 287 (2007).
[27] J. Zimmermann, B. A. Camley, W.-J. Rappel, and H. Levine, Proceedings of the National Academy of Sciences **113**, 2660 (2016).
[28] B. Szabó, G. J. Szöllösi, B. Gönci, Z. Jurányi, D. Selmeczi, and T. Vicsek, Physical Review E **74**, 061908 (2006).
[29] S. Henkes, Y. Fily, and M. C. Marchetti, Physical Review E **84**, 040301 (2011).
[30] A. Puliafito, L. Hufnagel, P. Neveu, S. Streichan, A. Sigal, D. K. Fygenson, and B. I. Shraiman, Proceedings of the National Academy of Sciences **109**, 739 (2012).
[31] See Supplemental Material for a complete mathematical description of the active athermal-local-yield-stress model and the GPU-Parallel Implementation.
[32] A. Puliafito, L. Hufnagel, P. Neveu, S. Streichan, A. Sigal, D. K. Fygenson, and B. I. Shraiman, Proceedings of the National Academy of Sciences **109**, 739 (2012).
[33] W. H. Herschel and R. Bulkley, Kolloid-Zeitschrift **39**, 291 (1926).
[34] E. Agoritsas, E. Bertin, K. Martens, and J.-L. Barrat, European Physical Journal E: Soft Matter **38**, 71 (2015).
[35] E. Agoritsas and K. Martens, "Nontrivial rheological exponents in sheared yield stress fluids," arXi [cond-mat.soft] (2016).

[36] L. Bocquet, A. Colin, and A. Ajdari, Physical Review Letters **103**, 036001 (2009).
[37] G. D'anna, P. Mayor, A. Barrat, V. Loreto, and F. Nori, Nature **424**, 909 (2003).
[38] K. J. Ford, J. F. Gilchrist, and H. S. Caram, Powder Technology **192**, 33 (2009).
[39] J. A. Dijksman, G. H. Wortel, L. T. H. van Dellen, O. Dauchot, and M. van Hecke, Physical Review Letters **107**, 108303 (2011).
[40] A. Pons, T. Darnige, J. Crassous, E. Clément, and A. Amon, EPL (Europhysics Letters) **113**, 28001 (2016).
[41] I. Theurkauff, C. Cottin-Bizonne, J. Palacci, C. Ybert, and L. Bocquet, Physical Review Letters **108**, 268303 (2012).
[42] S. Hilgenfeldt, S. A. Koehler, and H. A. Stone, Physical Review Letters **86**, 4704 (2001).
[43] A. Saint-Jalmes, Soft Matter **2**, 836 (2006).